The Effect of Pin Profiles and Process Parameters on Temperature and Tensile Strength in Friction Stir Welding of AL6061 Alloy

S. Emamian, M. Awang, F. Yusof, Patthi Hussain, Bahman Meyghani and Adeel Zafar

Abstract The main source of the heat generation during the Friction Stir Welding (FSW) is the friction force between tool and workpiece and the plastic deformation. The geometry of the tool including the pin and the shoulder highly affects the friction force. In this study, the effects of different pin profiles with different rotational and traversing speed are evaluated in order to obtain the optimum pin profile using heat generation and tensile strength. Three different rotational speed and welding speeds are applied with threaded cylindrical, conical, stepped conical and square pin profiles. Thermocouples K type have been embedded in order to record the temperature during the welding at the advancing and the retreating side. Moreover, tensile test and microstructure analysis are performed in order to study the microstructure. The results of experimental process and design of experiments are correlated well. The better joint produced with threaded cylindrical tool pin profile with rotation speed of 1600 rpm and welding speed of 40 mm/min.

Keywords FSW · Pin profile · Friction stir welding · Heat generation · Tensile strength

1 Introduction

Friction Stir Welding (FSW) was invented and patented by Thomas et al. at The Welding Institute (TWI) [1, 2]. There are three stages in the process plunging; welding stage and plunging out step. In the plunge stage, FSW tool which is made up of a pin and a shoulder, penetrates the plates. In some cases, there is a dwell time in which

S. Emamian · M. Awang (✉) · P. Hussain · B. Meyghani · A. Zafar
Department of Mechanical Engineering, Universiti Teknologi PETRONAS, Bandar Seri Iskandar, Malaysia
e-mail: mokhtar_awang@utp.edu.my

F. Yusof
Department of Mechanical and Manufacturing, University of Malaya, Kuala Lumpur, Malaysia

M. Awang (ed.), *The Advances in Joining Technology*, Lecture Notes in Mechanical Engineering, https://doi.org/10.1007/978-981-10-9041-7_2

the rotating tool remains at the plate without forward motion. In the welding stage, the rotating tool moves forward along the welding seam in order to form a weld bead [3, 4]. The schematic of FSW is shown in Fig. 1 [5].

Although all of the welding stages are significant, the significance of the plunging stage is more than other stages, because the main part of the heat will be generated at this stage and the workpiece will be affected extremely by high temperature and stresses [6]. It should be noted that most tool wear occurs during plunge stage due to the high load and flow stress [7, 8]. In FSW, the parameters that influence quality of joint and reduce tool wear are rotational speed and traverse speed while it was reported that the influence of the geometry of the tool is more than the abovementioned process parameters [9, 10]. The geometry of the tool is separated into two different parts of shoulder and pin whereby both have a significant effect on the material flow and the welding temperature. Among all shapes that scholars considered, some of them are not compared with each other in the literatures [11–21]. To illustrate, Patil and Soman [13] only utilized Tri-flute and taper screw during different welding speeds. In the same way, [16] investigated different pin profiles in which the square profile was absent. [22] studied the influence of the pin profiles and the shoulder diameter on the formation of FSW stirring zone. They found that the square pin profile with 18 mm shoulder diameter have better weld quality in comparison with other pin profiles. In other research, they investigated the influence of the different pin profiles and the welding speed during the FSW. Their results indicated that the square pin profile produced defect free weld compared to other pin profiles [12].

[23], studied the influence of different pin profiles on the metallurgical and mechanical properties of Al-Metal Matrix Composite. They concluded that the square pin profile has better tensile strength in comparison with other pin profiles. However, the threaded cylindrical was not involved in their study. [24], investigated the effect of the different pin profiles on the mechanical properties of FSW of pure copper. Their results showed that the square pin profile have higher mechanical properties and better grain structure in comparison with the threaded cylindrical.

There are many considerable experimental and numerical studies on FSW of different alloys. [25] comprehensively reviewed the friction stir processes. [26] reviewed

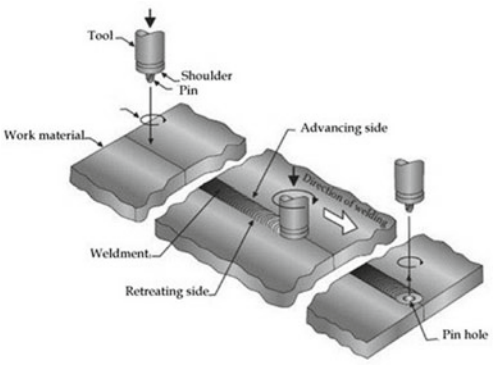

Fig. 1 Schematic of friction stir welding [3]

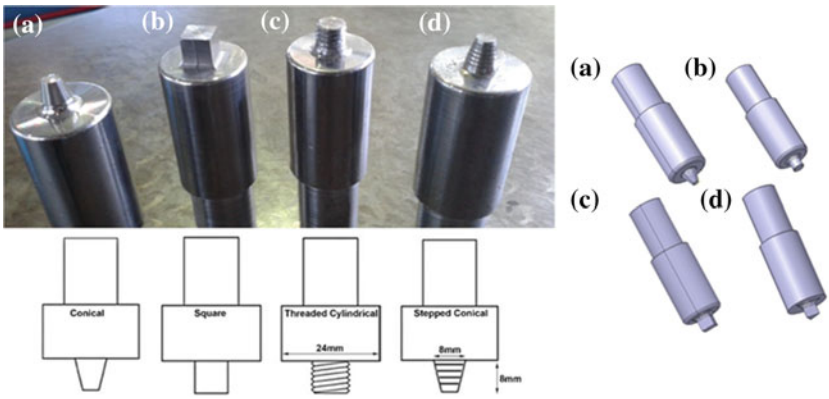

Fig. 2 Different pin profiles. **a** Conical. **b** Square. **c** Threaded cylindrical. **d** Stepped conical

the structure and the properties of FSW. [27] gave a broad review of numerical analysis of FSW. [28] reviewed the different pin profiles. [29] studied finite element modeling approach for Friction Stir Spot Welding (FSSW) on Al6061. They applied adaptive mesh to reduce the high distortion during simulation. Besides, [30] considered the plunge stage using numerical modeling and experimental. They utilized Al2024 alloy for the experiment.

The critical part of FSW is the pin profile, because it affects the welding quality. Therefore, regarding the review of literature, in this paper, four FSW tool pin profile have been selected including; square (s), threaded cylindrical (TC), stepped conical (SC), and conical (C). Figure 2 shows the schematic of profiles.

An appropriate design of the tool (especially the pin profiles) is able to generate proper heat and mixing the plasticized materials. Another significant factor which affects the heat generation is the process parameters such as rotating speed, traveling speed [25]. In this paper, in order to optimize the pin profile of FSW tool and process parameter during FSW, the thermomechanical behavior of the welded samples has been studied in detail.

2 Methodology

2.1 Experimental Set up

As mentioned earlier, four different pin profiles were selected for experiments. The heat treated H13 steel was used as the tool material and the workpiece AA6061-T6 with the dimension of 100 mm × 100 mm × 10 mm has been clamped. The chemical composition of a workpiece and the tool is shown in Table 1.

Table 1 Chemical composition and mechanical properties of base metal and the tool

AA6061-T6	**Chemical composition %—workpiece**								
	Mg	Cr	Ti	Zn	Mn	Fe	Si	Cu	Al
	0.98	0.19	0.05	0.01	0.07	0.3	0.47	0.23	Balanced
	Mechanical properties								
	UTS (Mpa)	Yield Strength (Mpa)	Elongation (%)						
	305	253	12						
H13	**Chemical composition %—tool**								
	C	Si	Mn	Cr	Mo	V	P	S	Fe
	0.4	0.92	0.34	5.07	1.25	0.95	0.019	0.001	Balanced

The experiments were performed by FSW-TS-F16 friction stir welding device host machine. The single pass welding procedure has been used to fabricate the joints. The heat treatment operation is done on the FSW tool. The first step of the heat treatment is preheating cycle. According to the standard, ASTM E8 temperature for preheating is around 760 °C, held for 15 min. Then, it is soaking cycle in the austenite formation zone in which the temperature is raised up to 1010 °C and held for 30 min. After the soaking cycle, the tool is removed from the furnace and cooled to 65 °C, when the furnace has reached a temperature of 565 °C, the tools are allowed to a temper for 2 h [31]. Three rotational speeds and three traverse speeds were selected to evaluate the temperature during different speeds that are listed in Table 2. In order to record the temperature during the welding, thermocouples (K type) are embedded in the advancing side and retreating sides with the specified distance. Figure 3 shows the position of the thermocouples.

Table 2 Welding parameters and tool dimension

Process parameters	Values
Rotational speed (rpm)	800, 1200, 1600
Traveling speed (mm/min)	40, 70, 100
Axial force (kN)	7
Pin length (mm)	8
Tool shoulder diameter (mm)	24
Pin diameter (mm)	8

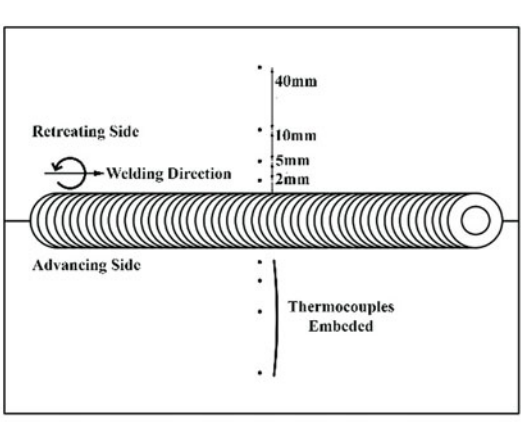

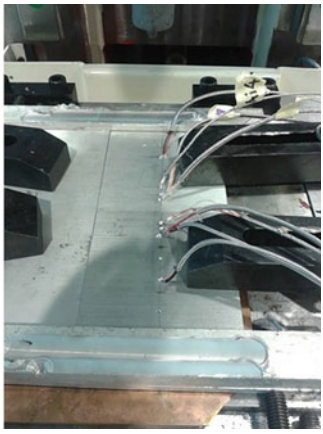

Fig. 3 Workpiece and thermocouples position

2.2 Microstructure Analysis

Microstructure analysis of FSW joints is performed as per ASTM to optimize the tool pin profile. In order to cut the samples, a wire cut machine has been used.

Then, the samples are grinded to remove material deformed produced from sectioning. Grinding process is followed by the polishing process. Polishing is removing the scratches from the surface of specimens to prepare them for the etching process. In order to perform etching, the specimens are immersed into Keller's reagent for 10–20 s. The chemical composition of Keller's reagent are listed in Table 3 [32, 33].

2.3 Tensile Test

Tensile test is performed using a universal testing machine 50KN Amsler HA50 with standard ASTM: E8/E8M with constant crosshead speed of 0.9 mm/min. Tensile testing is a fundamental material science test that is subjected to a controlled tension force until the fracture. The results from the test are commonly used to select a material for an application, to control the quality of the weld, and also to predict the fraction of the material under different types of forces. Properties that are directly measured during a tensile test are ultimate tensile strength, maximum elongation and reduction in area. Tensile test performed using a universal testing machine with standard ASTM: E8/E8M utilized for tensile and performed with constant crosshead speed of 0.9 mm/min. Figure 4 shows the schematic of tensile samples for the test according to ASTM E8.

Table 3 Chemical composition of Keller's reagent

Keller's reagent				
Composition	HF	HCl	HNO_3	Water
Volume (ml)	2	3	5	190

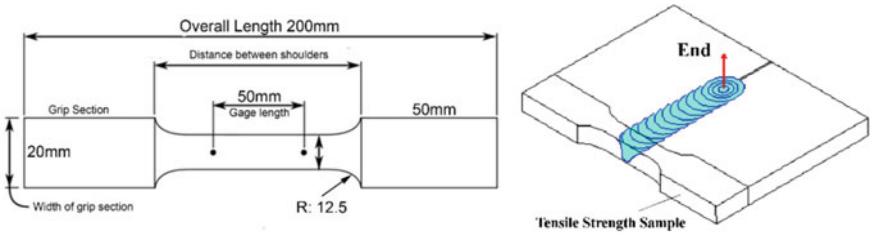

Fig. 4 Schematic of tensile test sample and dimension

2.4 Design of Experiment (DOE)

Design of experiments (DOE) is a systematic method in order to determine the relationship between factors affecting in a process and also to find the cause-and-effect relationships. Basically, DOE is a statistical technique for analyzing and organizing the experiments [34]. In DOE, the factors comprise of different parameters which are controlled by researchers, meanwhile the responses make up the dependent variable, which in this case, refers to productivity. To implement a DOE technique, some steps need to be followed such as: choosing the factors and their levels, choosing a response variable, choosing the experimental design, performing the experiments, analyzing the data, and promoting the best option [35].

In this research, the general factorial design has been selected for evaluating the effect of the several parameters on the heat generation and peak stress. In the first step for conducting the results. Table 4 and Table 5 show the factors and their levels for the heat generation and the stress respectively.

Table 4 Factors and levels for heat generation

Factors	Levels			
Pin profile (A)	1	2	3	4
	Square	Threaded cylindrical	Stepped conical	Conical
Rotational speed—rpm (B)	800, 1200, 1600			
Welding speed—mm/min (C)	40, 70, 100			

Table 5 Factors and levels for peak stress

Factors	Levels			
Pin profile (A)	1	2	3	4
	Square	Threaded cylindrical	Stepped conical	Conical
Rotational speed—rpm (B)	800, 1600			
Welding speed—mm/min (C)	40, 100			

3 Results and Discussion

3.1 Heat Generation

Investigation of the heat generation in FSW is a complicated phenomenon and needs to be compared with the experimental data. In this study, heat generation of different parameters such as rotational speed, welding speed and tool pin profiles are investigated. Figure 5 illustrates the results of heat generation during FSW for advancing and retreating sides. These histograms show the maximum temperature from eight thermocouples for 36 sample welds. Highest temperature obtained from rotation speed of 1600 rpm for all pin profiles. For instance, for the threaded cylindrical tool pin profile, as the welding rotation speed increases from 800 to 1600 rpm, the temperature increases from 247.95 to 357.14 °C.

The Figure shows the relation of different parameters. As the welding increases from 40 mm/min to 100 mm/min, the temperature drops from 357.14 to 247.95 °C. This happens due to the reduced heat input per unit length and dissipation of heat over a wider region of workpiece at higher welding speed. On the other hand, by increasing the rotation speed, temperature would be increased. As the welding rotation speed increases from 800 to 1600 rpm, the temperature increases from 203 to 459.6 °C for the threaded cylindrical tool pin profile in the advancing side. This happens due to friction between tool and workpiece that generate more heat. Moreover, surface area of the tool effects heat generation. In this study, square pin profile produced a higher temperature around 460 °C due to its surface shape that creates more friction during FSW.

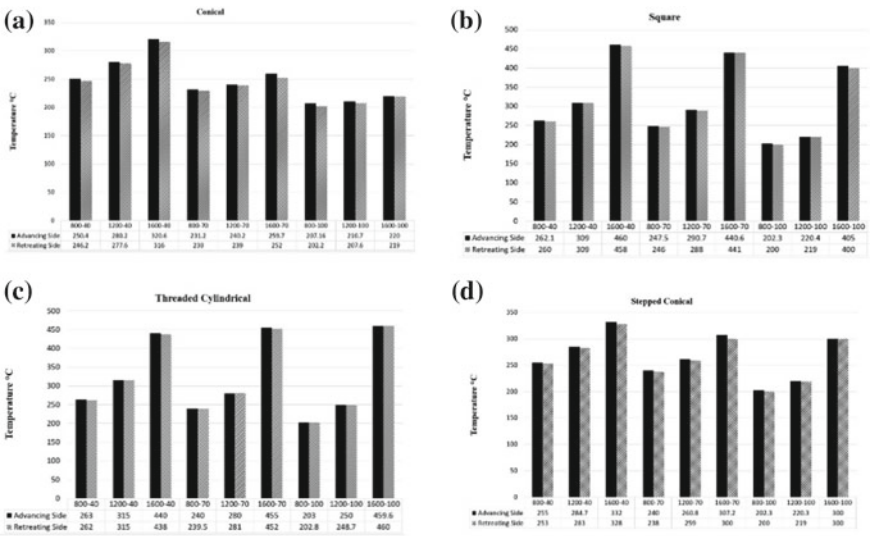

Fig. 5 Maximum temperature for different pin profiles

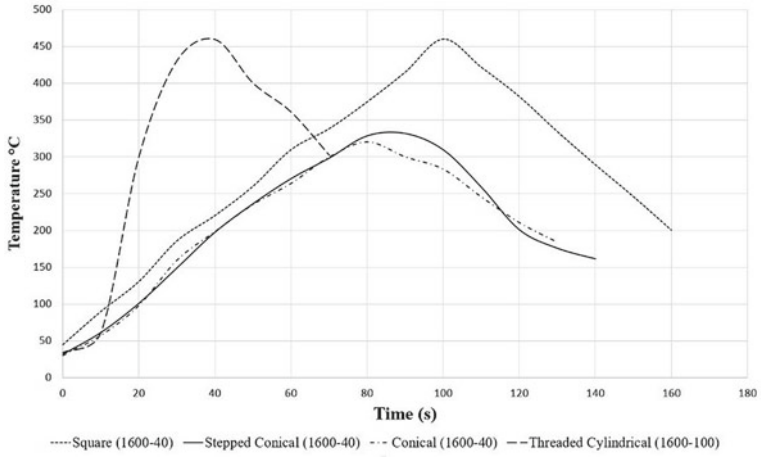

Fig. 6 Temperature graphs from different pin profiles

Advancing side in FSW process is the location from where the solid material starts to transform into semi-solid one and flows around the tool pin plunged into the material. The semi-solid material retreated and cooled in the retreating side. Therefore, advancing side has more solid state nature at any point of time/location compare to retreating side during FSW process. Therefore, advancing side should generate higher friction stress (unbalanced frictional force) which ultimately generates more heat and raises the peak temperature. Moreover, advancing side produced higher temperatures in comparison with retreating side due to pushing the material at the first connection and forwarding it to retreating side.

Temperature under the shoulder is higher due to high energy density. The peak of the temperature is about 80% of the material melting point 582–652 °C. From 36 welded samples, those where generates highest temperatures compared with each other to analyze heat generation during FSW with different pin profiles. Figure 6 shows the combined graphs. As can be seen in the Figure, square pin profile produced a higher temperature around 450 °C due to its surface shape that creates more friction during FSW.

During the welding process, the shoulder was the same, but pin profiles changed with different speeds. We could obtain different temperatures from different speeds. However, the graphs show that differences between peak temperatures of samples welded by different pin profiles are very little and not significant. According to Eqs. (1) and (2), pin profile affects heat generation.

$$Q_1 = 2/3\,\pi\,\tau_{contact}\,\omega\left(R^3_{shoulder} - R^3_{pin}\right)(1 + tan_\alpha) \tag{1}$$

$$Q_2 = 2\,\pi\,\tau_{contact}\,\omega R^2_{pin} H_{pin} \tag{2}$$

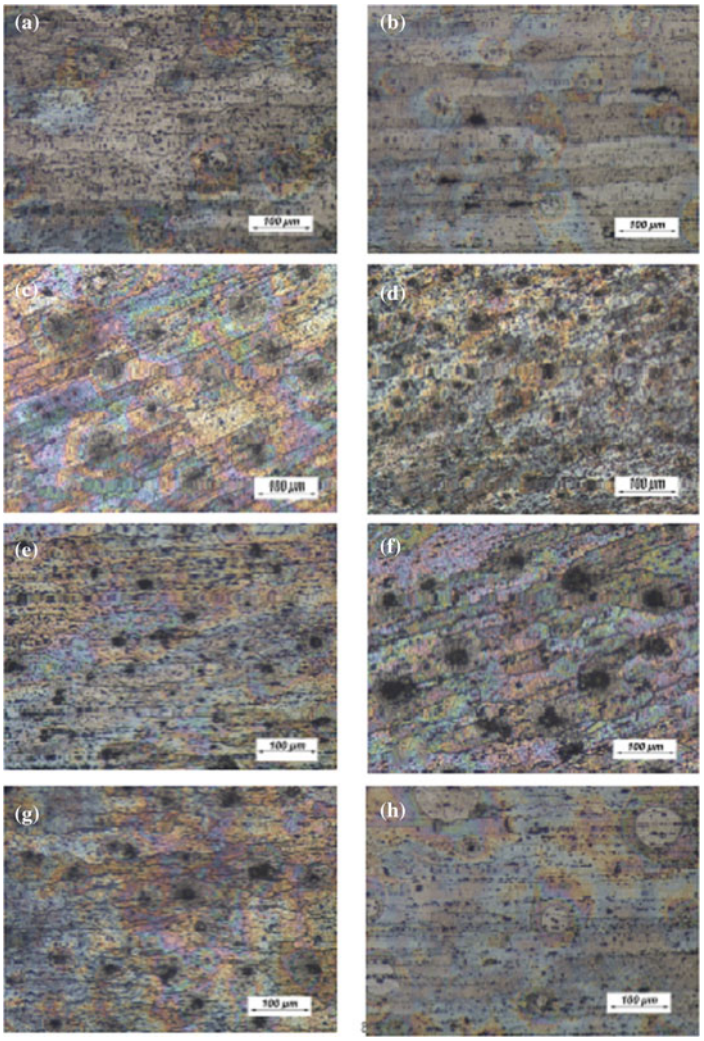

Fig. 7 Microstructure of advancing and retreating side. **a** Advancing side of stepped conical pin profile. **b** Advancing side of conical pin profile. **c** Advancing side of threaded cylindrical pin profile with rotation speed of 1600 rpm and welding speed of 100 mm/min. **d** Advancing side of threaded cylindrical pin profile with rotation speed of 800 rpm and welding speed of 40 mm/min. **e** Retreating side of stepped conical. **f** Retreating side of conical pin profile. **g** Retreating side of threaded cylindrical with rotation speed of 1600 rpm and welding speed of 100 mm/min. **h** Retreating side of threaded cylindrical with rotation speed of 800 rpm and welding speed of 40 mm/min

Equations (3) and (4) give the local heat generation rate due to friction and deformation work respectively.

$$de_f = \delta\,(r\omega - U\,sin\,\theta)\,\mu_f\,p\,dA \tag{3}$$

$$de_s = (1-\delta)\,(r\omega - U\,sin\,\theta)\,\tau_y\,dA \tag{4}$$

where δ is the extent of the slip, μ_f is the friction coefficient, μ_s is the shear yield stress and p is the local pressure applied by the tool on the elemental area dA. When δ is 1, no material sticks to the tool and all the heat is generated by friction. In contrast, when $\delta = 0$, work-piece material sticks to the tool and all the heat is generated by plastic deformation [36, 37].

According to the results of the experiment, higher temperature is generated from higher rotational speed and lower temperature comes from lower traverse speed. Therefore, increasing the rotational speed will increase the temperature and increasing the welding speed will reduce temperature that proved with other researches that studied in literature review. Moreover, the highest temperature is from a square pin profile that can be demonstrated with its surface area connection with the materials.

3.2 Microstructure Analysis

The etched specimens are examined using optical microscope Leica MC170 HD and the grain size of the cross section of the joints are analyzed. The cut specimens are immersed into Keller's reagent for 10–20 s for the etching process. Finally, Scanning Electron Microscope (SEM) is used in order to investigate the microstructure.

It is notable that all microstructures of threaded cylindrical are homogenous and there are no significant differences between advancing and retreating side. Due to utilizing threaded shapes during FSW mixing of the materials is higher and also the grain size is better. The role of the pin profile for making the microstructure is not inevitable. The results showed that, the threaded cylindrical made a homogeneous microstructure in FSW in comparing with conical and stepped conical profiles. During FSW, the temperature variation is very high, therefore, the recrystallization of samples is not complete and are broken or are in the shape of a pancake. As per discussion earlier about the heat generation by increasing the rotational speed, the temperature is also increased and thus, the microstructure should be coarse. On the other hand, by increasing the welding transverse speed, the temperature falls down and thus the microstructure is finer.

A comparison between different microstructures at the stir zones in advancing and retreating sides under the various FSW conditions is shown in Fig. 7a–h. Figures (a) and (b) are related to advancing and retreating side of the conical profile with rotation speed of 1600 rpm and welding speed of 40 mm/min. Figures (c) and (d) are microstructure of square profiles. Threaded cylindrical shown in figures (e) and (f) and stepped conical is shown with figures (g) and (h). The results indicated that the

Table 6 Grain size of joints in various samples

Pin profile	Rotational speed (rpm)	Welding speed (mm/min)	Grain size (μm)	
			AS	RS
Stepped conical	800	100	38.9	34.7
Conical	800	40	49.3	43.3
Threaded cylindrical	1600	100	32.26	31.8
Threaded cylindrical	800	40	39.8	33

microstructure of the sample with rotational speed of 1600 rpm with 100 mm/min welding speed is finer.

As per discussion earlier about heat generation by increasing rotational speed, temperature would be increased. Therefore, the microstructure should be coarse. On the other hand, by increasing the welding speed, temperature falls down and microstructure would be coarse again. Table 6 indicates the grain sizes.

The role of pin profile for making the microstructure is not inevitable. Threaded cylindrical made a homogeneous microstructure in FSW in comparing with conical and stepped conical profiles.

In comparing with mechanical test and heat generation, sample with rotational speed of 1600 rpm with 100 mm/min welding speed produced sounds joint with finer microstructure.

3.3 Tensile Strength Analysis

After analyzing the microstructure, as can be seen in Fig. 8 some of the samples produced wormholes, therefore among 36 samples only 11 samples are Defect-free, and were selected for the tensile test. As mentioned earlier, these samples were tested using a universal testing machine with standard ASTM: E8/E8M utilized for tensile and performed with constant crosshead speed of 0.9 mm/min. Transverse tensile properties of FSW joints such as yield strength, tensile strength, and percentage of elongation have been evaluated. Table 7 illustrates the mechanical properties of selected samples. In another aspect, primary parameters such as welding speed has a significant role in tensile properties.

As shown, maximum tensile strength (73.91% of parent material) is observed in that specimen in which the threaded cylindrical profile with rotational speed of 1600 rpm and welding speed of 100 mm/min is used. In contrast, the inferior properties belong to conical pin profile with the rotational speed of 800 rpm and the transverse speed of 40 mm/min. Therefore, lower tool rotational speeds produced insufficient intermixing. Thus, the mechanical strength will decrease at lower rota-

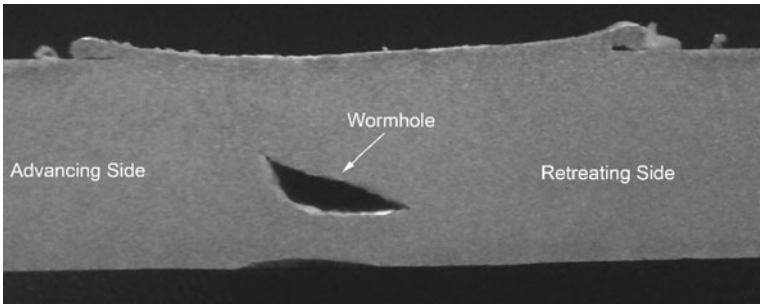

Fig. 8 Wormhole in FSW samples

Table 7 Tensile properties of 11 samples

Samples	0.2% yield strength	Tensile strength (MPa)	Elongation %
Conical (800-40)	113.50	180.45	6.25
Stepped conical (800-100)	129.70	188.21	5.10
Threaded cylindrical (800-40)	112.02	200.70	8.6
Threaded cylindrical (800-70)	125.63	212.22	7.66
Threaded cylindrical (800-100)	130.76	213.17	5.14
Threaded cylindrical (1200-40)	112.30	201.23	8.84
Threaded cylindrical (1200-70)	124.32	210.04	7.87
Threaded cylindrical (1200-100)	131.50	193.84	3.88
Threaded cylindrical (1600-40)	109.91	186.39	5.85
Threaded cylindrical (1600-70)	121.32	208.21	8.67
Threaded cylindrical (1600-100)	132.77	230.359	5.78

tional speeds [38]. Moreover, it is observed that by increasing the welding speed, tensile strength will be increased. In another aspect, primary parameters such as welding speed have a significant role in the tensile properties.

Table 8 shows the tensile properties of those specimens in which maximum heat is generated. These results showed that increasing the rotation speed can increase temperature. On the other hand, by reducing the welding transverse speed temperature is also increased.

Table 8 Tensile properties of FSW joints with maximum heat generation

Samples	0.2% yield strength	Tensile strength (MPa)	Elongation %
Conical (1600-40)	113.50	141.246	5.68
Square (1600-40)	129.70	104.841	2.213
Threaded cylindrical (1600-100)	132.77	230.359	5.78
Stepped conical (1600-40)	125.63	140.458	7.66

3.4 Design of Experiments Analyzes

3.4.1 Statistical Analysis for Heat Generation and Peak Stress

After choosing the factors, levels and the experimental parameters, data collection needs to be conducted by doing the experiments. As mentioned earlier by using general factorial design method, 36 conditions for the heat generation and 16 experiments for the peak stress are optimized. In order to decrease potential errors, two replicates for the heat generation and the peak stress is assumed. Therefore, as can be seen in Table 9 the numbers of the experiments for heat generation is equal to 72 (The number of experiments = 4 * 3 * 3 * (2 replicates) = 72).

As illustrated in Table 10, the number of the experiments for peak stress is equal to = 4 * 2 * 2 * (2 replicates) = 36.

3.4.2 Determining of Significant Factors for Heat Generation

In this study, Expert-design software is used for conducting statistical analyses. The result of ANOVA for the heat generation and the peak stress are presented in Table 11. Basically, *P*-value is a significant parameter that is usually used to identify the statistically significant factors due to it has influenced the final responses. It should be noted that, whenever *P*-values are less than 0.05, factors should be considered as significant. In contrast, when *P*-values are more than 0.05, it should be assumed as an insignificant factor [39]. Based on Table 5, the Model, F-value of 6526.42 implies that the model is significant. In addition, the *P*-values is less than 0.0500 which indicate the model terms are significant. In this case A, B, C, AB, AC, BC, ABC are significant model terms.

Table 12 verifies the accuracy of the model. As can be seen in the table, The "Pred R-Squared" of 0.9994 is in reasonable agreement with the "Adj R-Squared" of 0.9997. "Adeq Precision" measures the signal to noise ratio that a ratio greater than 4 is desirable. So ratio of 262.871 indicates an adequate signal.

Table 9 Result of Experiments for heat generation

Run	Pin profile (A)	Rotational speed—rpm (B)	Welding speed—mm/min (C)	Heat generation (°C)	
				Advancing side	Retreating side
1	Square	800	40	262.1	260
2	Threaded cylindrical	800	40	263	262
3	Stepped conical	800	40	255	253
4	Conical	800	40	250.4	246.2
5	Square	1200	40	309	309
6	Threaded cylindrical	1200	40	315	315
7	Stepped conical	1200	40	284.7	283
8	Conical	1200	40	280.2	277.6
9	Square	1600	40	460	458
10	Threaded cylindrical	1600	40	440	438
11	Stepped conical	1600	40	332	328
12	Conical	1600	40	320.6	316
13	Square	800	70	247.5	246
14	Threaded cylindrical	800	70	240	239.5
15	Stepped conical	800	70	240	238
16	Conical	800	70	231.2	230
17	Square	1200	70	290.7	288
18	Threaded cylindrical	1200	70	280	281
19	Stepped conical	1200	70	260.8	259
20	Conical	1200	70	240.2	239
21	Square	1600	70	440.6	441
22	Threaded cylindrical	1600	70	455	452
23	Stepped conical	1600	70	307.2	300
24	Conical	1600	70	259.7	252
25	Square	800	100	202.3	200
26	Threaded cylindrical	800	100	203	202.8
27	Stepped conical	800	100	202.3	200
28	Conical	800	100	207.16	202.2
29	Square	1200	100	220.4	219
30	Threaded cylindrical	1200	100	250	248.7
31	Stepped conical	1200	100	220.3	219
32	Conical	1200	100	210.7	207.6
33	Square	1600	100	405	400
34	Threaded cylindrical	1600	100	459.6	460
35	Stepped conical	1600	100	300	300
36	Conical	1600	100	220	219

Table 10 Result of experiment for peak stress

Run	Pin profile (A)	Rotational speed—rpm (B)	Welding speed—mm/min (C)	Peak stress (MPa)	
				Advancing side	Retreating side
1	Conical	800	40	121.414	135
2	Stepped conical	800	40	178.561	160
3	Square	800	40	117.496	123
4	Threaded cylindrical	800	40	200.709	213
5	Conical	1600	40	141.246	161
6	Stepped conical	1600	40	140.458	149
7	Square	1600	40	104.841	123
8	Threaded cylindrical	1600	40	186.392	196
9	Conical	800	100	170.94	176
10	Stepped conical	800	100	188.218	225
11	Square	800	100	153.274	143
12	Threaded cylindrical	800	100	213.73	230
13	Conical	1600	100	180.456	173
14	Stepped conical	1600	100	131.943	138
15	Square	1600	100	136.556	125
16	Threaded cylindrical	1600	100	230.359	245

Table 11 ANOVA result for heat generation

Source	Sum of square	DF	Mean square	F value	*P*-value	Remarks
Block	14.07	1	14.07			
Model	4.376E+005	35	12502.97	6526.42	<0.0001	Significant
A	76208.97	3	25402.99	13260.09	<0.0001	Significant
B	2.313E+005	2	1.157E + 005	60378.54	<0.0001	Significant
C	42508.87	2	21254.43	11094.59	<0.0001	Significant
AB	80365.51	6	13394.25	6991.66	<0.0001	Significant
AC	2262.53	6	377.09	196.84	<0.0001	Significant
BC	1475.16	4	368.79	192.50	<0.0001	Significant
ABC	3328.41	12	277.37	144.78	<0.0001	Significant
Residual	67.05	35	1.92			
Lack of Fit	67.05	34	1.97			
Pure Error	0.000	1	0.000			
Cor Total	4.377E+005	71				

Table 12 Model accuracy

Std. Dev.	1.38	R-squared	0.9998
Mean	286.88	Adj R-squared	0.9997
C.V.	0.48	Pred R-squared	0.9994
Press	284.21	Adeq precision	262.871

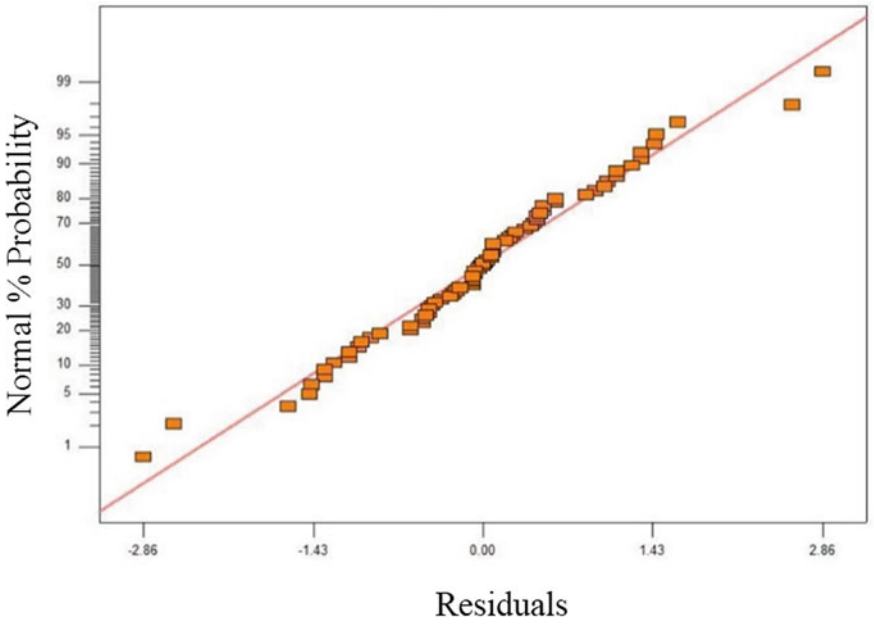

Fig. 9 Normal plot of residual

3.4.3 Residual Analysis

The residual versus predicted value and normal probability plots are two significant graphical approaches that were used in order to check the validity of the regression model [40]. The results of the residual versus predicted value shows that the difference between the predicted values and the observed values. If the residuals have a regular pattern, it will infer that the suggested model is not adequate. Moreover, residuals in normal probability plot should be laid in a straight line [41]. As can be seen in Fig. 9, the straight line confirms that the model is adequate and correct. Moreover, the structure less pattern of the residual versus predicted value confirms that the developed model is adequate (Fig. 10).

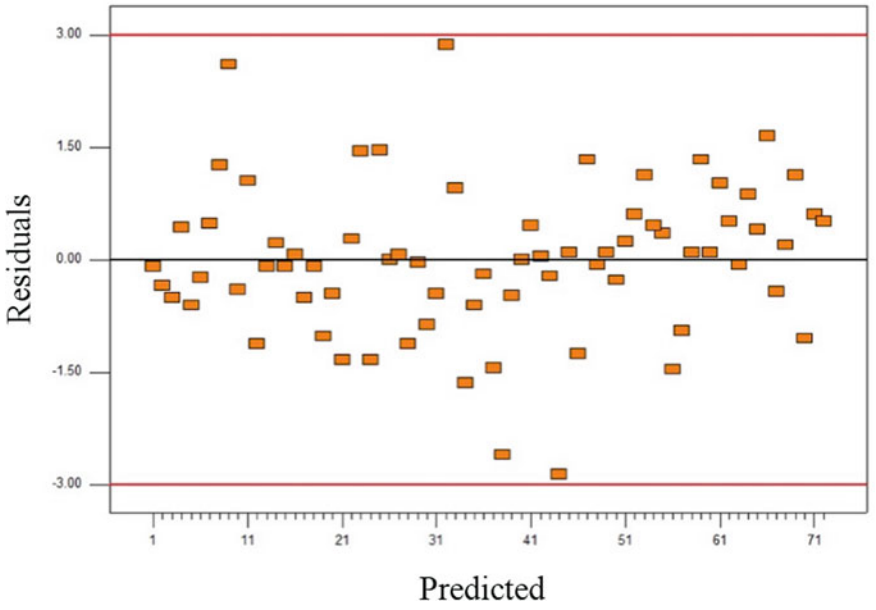

Fig. 10 Residual versus predicted value

3.4.4 Peak Stress

Determining of Significant Factors

Table 13 shows the result of ANOVA for the peak stress. As can be seen, factors A, B, C and interactions AB and ABC are significant and have a considerable effects on the peak stress.

Tabel 14 indicates that the "Pred R-Squared" of 0.8533 is in reasonable agreement with the "Adj R-Squared" of 0.9355. Also "Adeq Precision" measures the signal to noise ratio that a ratio greater than 4 is desirable. So ratio of 18.276 reveals an adequate signal.

3.4.5 Residual Analysis for Peak Stress

As can be seen in Fig. 11, the straight line confirms that the model is adequate and correct. Moreover, the structure less pattern of the residual versus predicted value confirms that the developed model is adequate and has a constant error (Fig. 12).

Table 13 ANOVA result for peak stress

Source	Sum of square	DF	Mean square	F value	Prob > F	Remarks
Block	438.13	1	438.13			
Model	43647.15	15	2909.81	30.01	< 0.0001	Significant
A	30756.93	3	10252.31	105.75	< 0.0001	Significant
B	1093.85	1	1093.85	11.28	0.0043	Significant
C	5236.71	1	5236.71	54.02	< 0.0001	Significant
AB	4155.39	3	1385.13	14.29	0.0001	Significant
AC	546.39	3	182.13	1.88	0.1766	Notsignificant
BC	267.99	1	267.99	2.76	0.1171	Notsignificant
ABC	1589.90	3	529.97	5.47	0.0097	Significant
Residual	1454.20	15	96.95			
Cor total	45539.48	31				

Table 14 Model accuracy for peak stress

Std. Dev.	9.85	R-squared	0.9678
Mean	165.99	Adj R-squared	0.9355
C.V.	5.93	Pred R-squared	0.8533
Press	6618.24	Adeq precision	18.276

3.4.6 Optimum Condition

The results of experiment and design of experiments have a good correlation. In most samples, advancing side produced higher temperature. Higher temperature obtained from square pin profile as discussed earlier due to its shape and geometry of contact area. However, from the experiments, we found that threaded cylindrical produced higher quality joints. It is observed that in some cases that temperatures are not exactly the same as DOE results because of some technical errors while getting temperature from thermocouples. Moreover, the results indicated that the highest tensile strength comes from threaded cylindrical with rotation speed of 1600 rpm and welding speed of 100 mm/min.

For the heat generation, the actual factor for the welding speed is obtained at 100 mm/min. Table 15 indicates the optimum parameters for heat generation and peak stress. The maximum temperature was 459.8 °C for the threaded cylindrical and rotation speed of 1600 rpm. Moreover, the stress of 237.68 MPa is obtained for threaded cylindrical.

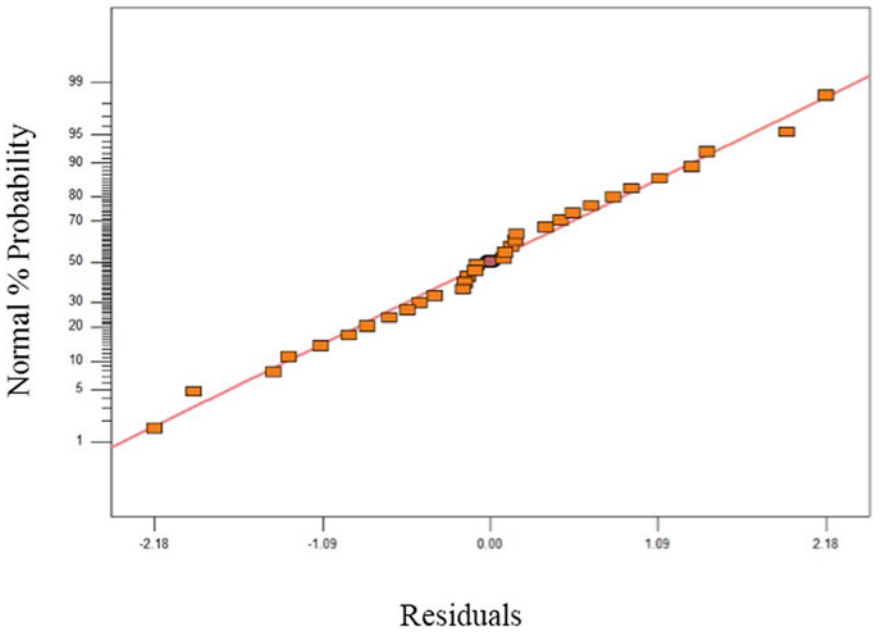

Fig. 11 Normal plot of residuals

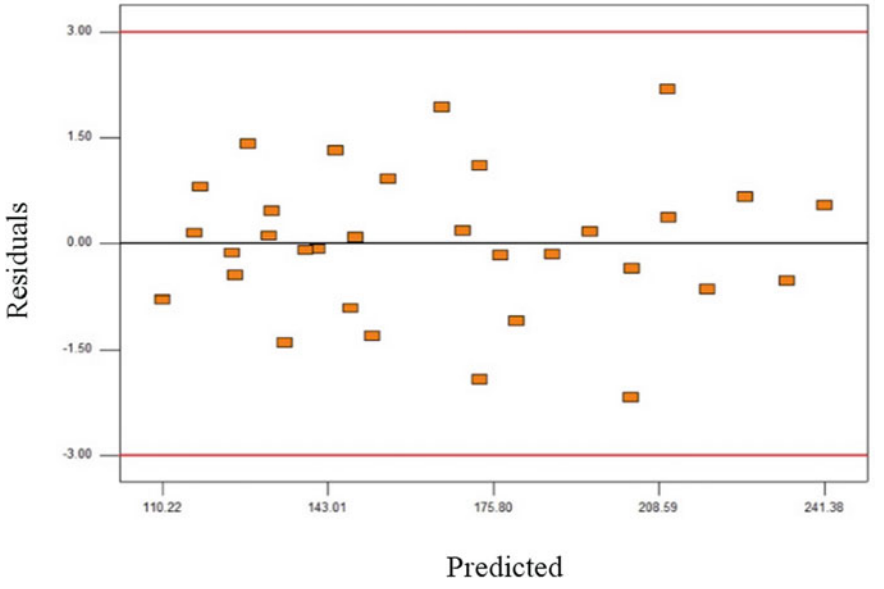

Fig. 12 Residual versus predicted value

Table 15 Optimum parameters from DOE

Heat generation					
Optimum parameters	Pin profile	Rotation speed (rpm)	Welding speed (mm/min)	Temperature (°C)	Desirability
	Threaded Cylindrical	1600	100	459	0.99
Peak stress					
Optimum parameters	Pin profile	Rotation speed (rpm)	Welding speed (mm/min)	Stress(MPa)	Desirability
	Threaded cylindrical	1600	100	237.68	0.94

4 Conclusion

Experimental analyses and DOE are performed by different rotational and welding speeds with various pin profiles. During experimental step 11 samples are approved for further studies due to absence of weld defect.

- In regard to heat generation, the results of experimental and DOE are almost similar.
- Increasing the rotational speed will increase temperature. On the other hand, by increasing the welding speed, temperature comes down.
- Highest strength produced with higher rotational speed due to better intermixing of the materials during the welding process.
- In aspect of microstructure, With the increase of rotational speed, the welding speed grain size would be bigger. Moreover, pin profiles have an influence on the microstructure and grain size after welding.
- The results of experiments and DOE for heat generation, tensile test and microstructure analysis indicate that sounds joint produced with threaded cylindrical tool pin profile with rotation speed of 1600 rpm and welding speed of 100 mm/min.

Acknowledgements The authors would like to acknowledge Universiti Teknologi PETRONAS, Malaysia for the financial support under I-Gen grant (0153DA-135).

References

1. Thomas W et al International patent no. 1991, PCT/GB92/02203, GB Patent
2. Meyghani B et al (2017) Developing a finite element model for thermal analysis of friction stir welding by calculating temperature dependent friction coefficient. In: 2nd International conference on mechanical, manufacturing and process plant engineering. Springer, Berlin

3. Mandal S, Rice J, Elmustafa A (2008) Experimental and numerical investigation of the plunge stage in friction stir welding. J Mater Process Technol 203(1):411–419
4. Meyghani B et al (2017) A comparison of different finite element methods in the thermal analysis of Friction Stir Welding (FSW). Metals 7(10):450
5. Threadgill PL, Leoneard AJ, Shercliff HR, Withers PJ (2009) Friction stir welding of aluminium alloys. [cited 2014; Available from: http://www.twi-global.com/technical-knowledge/published-papers/friction-stir-welding-of-aluminium-alloys/]
6. Meyghani B, Awang M, Emamian S (2017) A mathematical formulation for calculating temperature dependent friction coefficient values: application in Friction Stir Welding (FSW). In: Defect and diffusion forum. Trans Tech Publ
7. Mandal S, Williamson K (2006) A thermomechanical hot channel approach for friction stir welding. J Mater Process Technol 174(1–3):190–194
8. Lienert T et al (2003) Friction stir welding studies on mild steel. Welding J-NY 82(1):1-S
9. Hajideh MR et al (2017) Investigation on the effects of tool geometry on the microstructure and the mechanical properties of dissimilar friction stir welded polyethylene and polypropylene sheets. J Manuf Process 26:269–279
10. Meyghani B, Awang M, Emamian S (2016) A comparative study of finite element analysis for friction stir welding application. ARPN J Eng Appl Sci 11:12984–12989
11. Elangovan K, Balasubramanian V (2007) Influences of pin profile and rotational speed of the tool on the formation of friction stir processing zone in AA2219 aluminium alloy. Mater Sci Eng, A 459(1–2):7–18
12. Elangovana K, Elangovana V (2008) Influences of tool pin profile and welding speed on the formation of friction stir processing zone in AA2219 aluminium alloy. Mater Process Technol 200(1–3):163–175
13. Patil H, Soman S (2010) Experimental study on the effect of welding speed and tool pin profiles on AA6082-O aluminium friction stir welded butt joints. Int J Eng Sci Technol 2(5):268–275
14. Xu W et al (2013) Influence of welding parameters and tool pin profile on microstructure and mechanical properties along the thickness in a friction stir welded aluminum alloy. Mater Des 47:599–606
15. Thube RS, Pal SK (2014) Influences of tool pin profile and welding parameters on Friction stir weld formation and joint efficiency of AA5083 Joints produced by Friction Stir Welding. Magnesium (Mg) 4:4.9
16. Motalleb-nejad P et al (2014) Effect of tool pin profile on microstructure and mechanical properties of friction stir welded AZ31B magnesium alloy. Mater Des 59:221–226
17. Trimble D, O'Donnell GE, Monaghan J (2015) Characterisation of tool shape and rotational speed for increased speed during friction stir welding of AA2024-T3. J Manuf Process 17:141–150
18. Ilangovan M, Rajendra Boopathy S, Balasubramanian V (2015) Effect of tool pin profile on microstructure and tensile properties of friction stir welded dissimilar AA 6061–AA 5086 aluminium alloy joints. Defence Technol 11(2):174–184
19. Krasnowski K, Hamilton C, Dymek S (2015) Influence of the tool shape and weld configuration on microstructure and mechanical properties of the Al 6082 alloy FSW joints. Arch Civil Mech Eng 15(1):133–141
20. Nadikudi BKB et al (2015) Formability analysis of dissimilar tailor welded blanks welded with different tool pin profiles. Trans Nonferrous Metals Soc China 25(6):1787–1793
21. Emamikhah A et al (2014) Effect of tool pin profile on friction stir butt welding of high-zinc brass (CuZn40). The Int J of Adv Manuf Technol 71(1):81–90
22. Elangovan K, Balasubramanian K (2008) Influences of tool pin profile and tool shoulder diameter on the formation of friction stir processing zone in AA6061 aluminium alloy. Mater Des 29(2):362–373
23. Vijay SJ, Murugan N (2010) Influence of tool pin profile on the metallurgical and mechanical properties of friction stir welded Al–10 wt.% TiB2 metal matrix composite. Mater Des 31(7):3585–3589

24. Khodaverdizadeh H, Heidarzadeh A, Saeid T (2013) Effect of tool pin profile on microstructure and mechanical properties of friction stir welded pure copper joints. Mater Des 45:265–270
25. Mishra RS, Ma ZY (2005) Friction stir welding and processing. Mater Sci Eng R: Rep 50(1–2):1–78
26. Nandan R, DebRoy T, Bhadeshia HKDH (2008) Recent advances in friction-stir welding—process, weldment structure and properties. Prog Mater Sci 53(6):980–1023
27. He X, Gu F, Ball A (2014) A review of numerical analysis of friction stir welding. Prog Mater Sci 65:1–66
28. Emamian S et al (2017) A review of friction stir welding pin profile. Springer, Berlin
29. Awang Mucino VH, Feng Z, David SA (2005) Thermo-mechanical modeling of Friction Stir Spot Welding (FSSW) process: use of an explicit adaptive meshing scheme. SAE technical paper, 2006. 1:1251
30. Mandal S, Rice J, Elmustafa AA (2008) Experimental and numerical investigation of the plunge stage in friction stir welding. J Mater Process Technol 203(1–3):411–419
31. William EB (2005) Heat treatment, selection, and application of tool steels, in heat treatment, selection, and application of tool steels. Carl Hanser Verlag GmbH & Co. KG., pp I–XV
32. ASTM E3-01 (2001) Standard practice for preparation of metallographic specimens. ASTM International, West Conshohocken
33. ASTM E407-07 (2015) Standard practice for microetching metals and alloys. ASTM International, West Conshohocken
34. Zahraee SM et al (2013) Combined use of design of experiment and computer simulation for resources level determination in concrete pouring process. Jurnal Teknologi 64(1):43–49
35. Sadeghifam AN et al (2015) Combined use of design of experiment and dynamic building simulation in assessment of energy efficiency in tropical residential buildings. Energy Build 86:525–533
36. Chen C, Kovacevic R (2003) Finite element modeling of friction stir welding—thermal and thermomechanical analysis. Int J Mach Tools Manuf 43(13):1319–1326
37. Zhang H, Zhang Z, Chen J (2005) The finite element simulation of the friction stir welding process. Mater Sci Eng, A 403(1):340–348
38. Rodriguez R et al (2015) Microstructure and mechanical properties of dissimilar friction stir welding of 6061-to-7050 aluminum alloys. Mater Des 83:60–65
39. Montgomery D (2009) Basic experiment design for process improvement statistical quality control. Wiley, USA
40. Zahraee SM et al (2014) Application of design of experiment and computer simulation to improve the color industry productivity: case study. Jurnal Teknologi 68(4):7–11
41. Zahraee SM et al (2014) Application of design experiments to evaluate the effectiveness of climate factors on energy saving in green residential buildings. Jurnal Teknologi (Sci Eng) 69(5):107–111